

Experimental Generation of ELF Radio Signals Using a Rotating Magnet

Hunter C. Burch, Alexandra Garraud, *Member, IEEE*, Michael F. Mitchell, Robert C. Moore, *Senior Member, IEEE*, and David P. Arnold, *Senior Member, IEEE*

Abstract—This article presents a simple, compact, low-power method for generating extremely low frequency (ELF) radio signals below ~ 500 Hz. This research is motivated by the prohibitively large size and low efficiency of conventional antennas operating in this frequency range. The successful generation of time-varying magnetic fields produced by the physical rotation of a 3 cm^3 permanent magnet is demonstrated. Ground plane and receiver orientation effects are analyzed both theoretically and experimentally. Observations as a function of distance from the source indicate that the fields are dominated by the static component, rather than by the radiation component, of the generated field. Based on these observations, the electromagnetic radiation emitted by a spinning magnet source is predicted to be weak. Nevertheless, static magnetic signaling using this technique is proven to be both possible and practical at frequencies below ~ 500 Hz and at distances in excess of 100 meters.

Index Terms—radio Transmitters, permanent magnets, magnetic field measurements

I. INTRODUCTION

Radio waves in the extremely low frequency (ELF, 3-3,000 Hz) band exhibit two propagation characteristics that are important for very practical applications: they can propagate to large distances around the globe with relatively low attenuation (~ 1 dB/1,000 km) and they can penetrate relatively deeply (10's of meters) into weakly conducting media, such as sea water [1-3]. The generation of propagating radio waves in the ELF band thus has important application for communications, navigation, and remote sensing at a global scale [4-8]. More localized applications—such as underground or underwater communication, position, navigation, and timing—could also benefit from the non-radiative near-fields produced by compact ELF sources.

It is difficult to efficiently excite ELF waves due in part to the extraordinarily large wavelengths (100-100,000 km) involved [9]. Magnetic loop antennas are typically considered to be poor ELF radiators due to their relatively low radiation resistance [9]. As a result, in the ELF frequency range, so-called "conventional" transmitters are anything but conventional. For example, the initial installation of the Siple transmitter at Siple Station, Antarctica in 1973 consisted of

two 23-km long crossed dipole antennas laid out horizontally on the ice [10]. Because the ice sheet was 2 km thick at that location (producing an effective elevation above ground near 2 km), the Siple transmitter was able to radiate ~ 100 W at 2 kHz with a $\sim 0.1\%$ radiation efficiency [10, 11]. To efficiently radiate at lower frequencies, below 100 Hz, special antenna geometries are required. Wait [2] theoretically evaluated and Project Sanguine implemented [12] an ELF transmitter below 100 Hz using $3,600\text{ km}^2$ of crossed horizontal wires with grounded tips. The grounded-tip concept requires large areas of low conductivity and leverages the resulting ground loops of electrical current to radiate at the desired ELF frequency with radiated power on the order of 1 W [2].

Due to the low efficiency and large resource requirements for conventional ELF transmission, generating ELF waves using unusual techniques is an active area of research. For example, naturally occurring electrical currents in Earth's lower ionosphere can be modulated so that they radiate in the ELF range. Modulated high-power radio wave heating of the lower ionosphere modifies the conductivity, and in turn modulates the electrical currents flowing in the region. Ionospheric heating experiments have been successfully performed at the HAARP [14], HIPAS [14], EISCAT [15], Arecibo [16], and SURA [17] facilities. In terms of radiated power, ELF waves (at 2125 Hz) generated by ionospheric heating using the HAARP facility were experimentally shown to produce 10-30 Watts of radiated power [18]. Signals at 575 Hz were somewhat lower in amplitude and were likely radiated at smaller power levels.

Each of the ELF generation techniques described above uses electrical currents as the field source and focuses on the generation of radiation fields. However, electrical currents are not the only possible method for generating an ELF wave. Dynamically moving electrical charges and/or magnetic dipoles can also be employed. For example, a permanent magnet, with no external power, can sustain a magnetic moment and produce a magnetic field equivalent to a solenoid carrying physical currents of several kiloamperes [19]. Physically rotating the magnet produces a time-varying magnetic field (or equivalently, accelerating charge), thereby generating an oscillating static magnetic field as well as a propagating electromagnetic wave. For example, spinning magnet transmitters have been previously simulated [20, 21], and low-data-rate communication has experimentally been demonstrated over distances < 1 m [22]. Arrays of spinning magnets are also being explored [23,24].

In comparison to these other recent publications, this article focuses on the experimental characterization of a rotating magnet transmitter in an outdoor environment over distances

Manuscript received on Feb. 20, 2018. This work was supported in part by the U.S. Department of Defense/DARPA under Contract HR00111820013.

All authors are with the University of Florida, Gainesville, FL 32611 USA (corresponding author: 352-392-4931; e-mail: darnold@ufl.edu).

Color versions of one or more of the figures in this communication are available online at <http://ieeexplore.ieee.org>.

Digital Object Identifier 10.1109/TAP.2016.xxx

of tens of meters. It is shown that the quasi-static magnetic near-field component is readily detectable at distances beyond 100 m for a simple centimeter-sized magnet rotated by an off-the-shelf motor. Practical issues associated with the orientation of the rotating transmitter are also investigated. These demonstrations experimentally confirm the utility and practicality of near-field signaling in the ELF band. The measurements also provide a baseline for future investigation of the feasibility of using spinning magnet dipoles to produce radiated power levels on the order of “conventional” ELF transmitters. While it may be physically difficult to produce Watts of radiated power using spinning magnets, attempting to do so using large volumes of rapidly spinning magnetic material is arguably less exotic than heating the Earth’s ionosphere, as in the case of HAARP.

Section II presents the experimental setup and procedures for generating and measuring ELF fields. Section III presents the experimental results along with extensive discussion. Conclusions and an outlook are provided in Section IV.

II. EXPERIMENTAL SETUP

In order to evaluate the efficacy of the spinning magnet method for ELF signal generation, a field test is performed using a spinning magnet ELF source and a magnetic loop antenna receiver. This section presents the implementation details for the experiments.

A. ELF Source

The ELF source comprises a cylindrical permanent magnet that is spun by an electrically powered hand-held rotary tool (Craftsman), as shown in Fig. 1. The magnet is a grade N42 Nd-Fe-B (K & J Magnetics, model RA2ADIA), with dimensions of 15.9 mm OD x 3.2 mm ID x 15.9 mm length (5/8” OD x 1/8” ID x 5/8” length), and a magnetic remanence $B_r = 1.3$ T. The magnet is magnetized diametrically, so that when rotated about its axis, it produces a rotating stray magnetic field. For a total magnet volume of 3 cm^3 , this corresponds to an equivalent magnetic dipole moment of $M_0 = (B_r / \mu_0) \cdot \text{VOL} = 3.1 \text{ A} \cdot \text{m}^2$. This dipole moment is substantially larger than the $0.4 \text{ A} \cdot \text{m}^2$ magnetic cylinder simulated in [21] and the three-magnet array with a net moment estimated to be $0.7 \text{ A} \cdot \text{m}^2$ evaluated in [24]. The magnet has an open bore, into which a steel shaft is press fit. The shaft is then mounted into the collet of the rotary tool. The rotary tool is powered by a standard 120 V_{AC} wall outlet (via ~60 m extension cord), and it rotates the magnet at speeds up to ~30,000 RPM (corresponding to ~500 Hz). The rotary tool is rated at 138 W.

B. Radio Receiver

The portable ELF receiver, shown in Fig. 2, consists of three orthogonal 1 Ω –1 mH square-loop antennas with a matched, low-noise amplifier for each channel. All three channels are recorded using a battery-powered Tascam data recorder with a 24-bit analog-to-digital converter and a 96 kHz sampling frequency. The complete receiver has a noise floor on the order of 1 fT/ $\sqrt{\text{Hz}}$ at 1 kHz (-55 dB-pT for the integration times used in this work) and a flat frequency response between 135 Hz and 45 kHz, meaning that the

output is proportional to the incident B-field in this frequency range. Amplitude calibration is performed by injecting controlled signals across the antenna terminals.

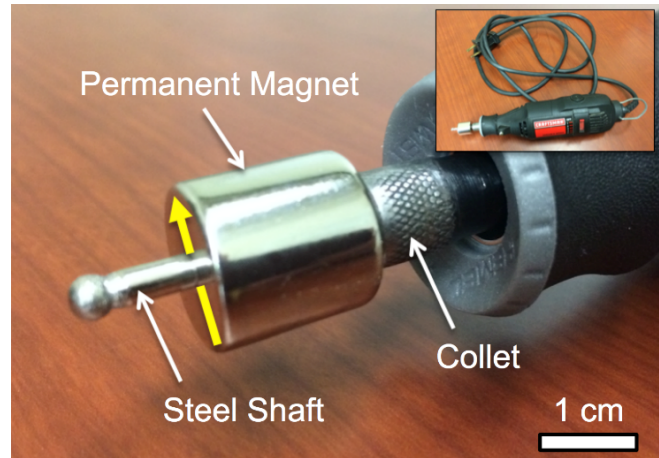


Fig. 1. A close-up picture of the magnet and rotary tool (inset); the arrow denotes the direction of the magnetic moment.



Fig. 2. The portable 3-axis magnetic field receiver.

C. Experimental Procedures

Measurements were performed on 8 August 2016 at Hume Field on the University of Florida campus (Gainesville, FL), as shown in Fig. 3. Hume Field is a flat, grassy recreational field away from roads and power lines. During the experiment, the ELF source remained stationary, positioned at one corner of the field, while the receiver was moved away from the source at intervals of ~9 m. At each location, approximately 1 min of data was recorded during which time

the rotary tool spun up, ran for approximately 30 s, and then spun down, so that each data file recorded both isolated background noise and the full spinning magnet ELF transmission. Data sets were also collected at both 9 m and 37 m with the rotary tool switched off (background) and with the rotary tool running without a magnet inserted. These control experiments confirm that the measured signals are predominantly generated by the spinning magnet, and not by the rotary tool or other interference sources.

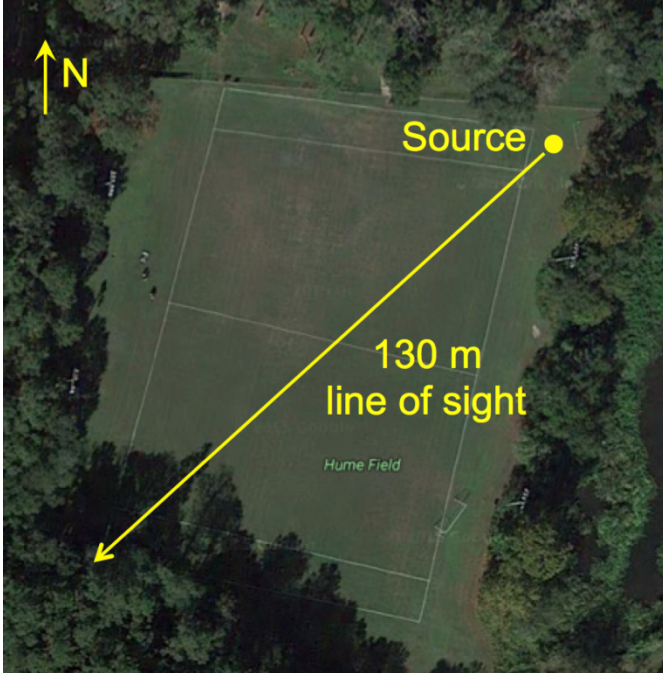


Fig 3. Test site on athletic field (Hume field) at the University of Florida.

For all experiments, the rotating magnet source was held by hand approximately 2.2 m above the ground. Except where noted, the axis of rotation of the magnet is vertical (i.e.

“lighthouse” orientation), as shown in Fig. 4a. However, for comparison, several additional experiments were conducted with the axis of rotation transverse to the line from the source to the receiver (i.e. “bulldozer” orientation), shown in Fig. 4b, in order to understand the directionality of the generated fields. Assuming the convention of a typical radio source, a cylindrical coordinate system (r, ϕ, z) is used with the origin placed at the source. Consequently, the x-coil is assumed to measure the radial field component B_r produced by the source; the y-coil, the azimuthal field component B_ϕ ; and the z-coil the vertical field component B_z .

From the recorded time-series data, spectrograms were calculated using the MATLAB `specgram` function. The data was segmented using a 2^{15} data-point (0.341 s) Hanning window with 90% overlap. Sample spectrograms are shown in Figs. 5, 6, and 8, which are calibrated to represent B-field strength (color) in dB relative to 1 pT (denoted dB-pT) as a function of time (x-axis) and frequency (y-axis). Because the background ambient environmental noise was typically around -35 dB-pT, the color scales in the spectrogram plots were clipped on the lower end to -20 dB-pT or -30 dB-pT for visual clarity. Vertical lines are associated with lightning flashes (impulsive signals), whereas the horizontal lines near multiples of 60 Hz are associated with the local power grid. In a typical experiment, the frequency of the generated B-field was observed to increase with time, settle near ~500 Hz for ~30 s, and then decrease as the rotary tool spins down. It is worth noting that the spindle speed of the handheld rotary tool is not very stable or precise, which leads to drift in the speed over the duration of the recording as well as some variation in average speed from test to test. The typical “steady-state” speed ranged from 490 Hz to 530 Hz.

To compare the signal amplitudes and relative phases generated in each case, a simple frequency-tracking filter was implemented to tightly follow the signals as a function of time. Amplitudes and phases were calculated by mixing down to baseband and low-pass filtering to a 0.5-Hz bandwidth. To

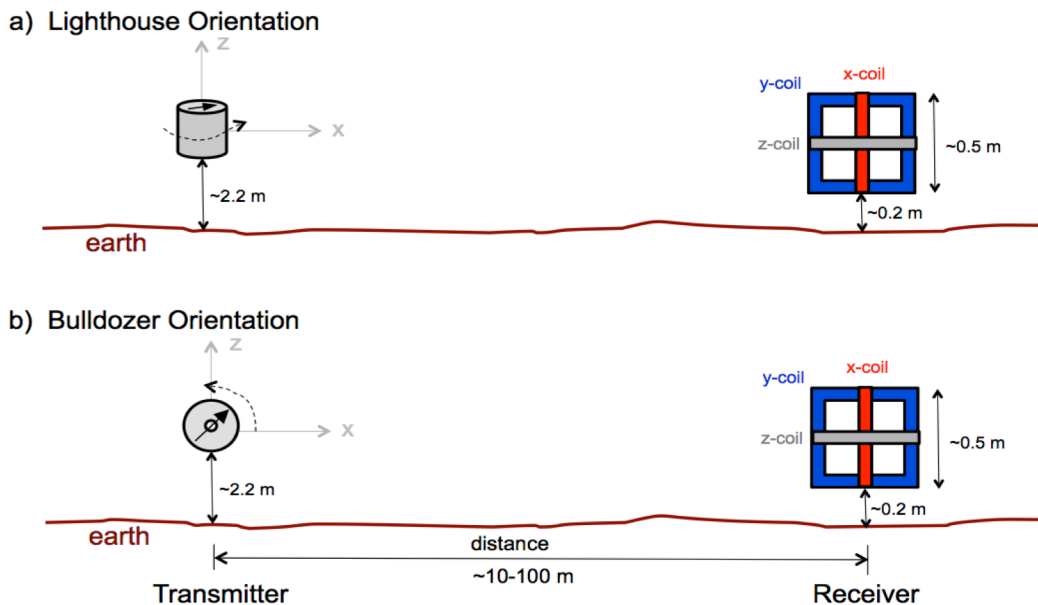


Fig. 4. Schematics of the orientation of the rotating magnet ELF source (in two different orientations) and the 3-axis receiver coils.

mitigate the effect of impulsive noise (due to lightning), the "steady-state" amplitudes and phases were sorted and the central 20% of data were averaged to produce impulse-free amplitude and phase measurements. Noise levels are assessed by repeating the signal processing using the same frequency-tracking filter with an offset of 30 Hz, so that only noise and none of the generated signal is within the pass band of the noise measurement. The reason for this "offset" approach is because the background noise is non-stationary and varies over consecutive trials.

III. EXPERIMENTAL RESULTS

The experimental results are presented in three sub-sections: (a) control experiments to confirm the measured signals are generated by the rotating magnet; (b) measurements of the signal amplitude vs. distance; and (c) comparison of different source orientations.

A. Control Experiments

In order to establish a baseline and to account for possible interference from the motor of the rotary tool, two control experiments were conducted at source-to-receiver distances of 9 m and 37 m. Example B_r measurements at 37 m are shown in Fig. 5 (similar results are obtained for B_θ and B_z , and also at 9 m distance). In Fig. 5, power line hum at multiples of 60 Hz have been falsely colored (covered) to improve visual clarity.

Fig. 5a shows the recorded data without the tool running; Fig. 5b shows the recorded signals with the motor running, but with no magnet inserted; Fig. 5c shows the data with the magnet installed in the tool. The signal ramp-up, steady-state

operation, and ramp-down are clearly observed in Fig. 5c. The background in-band noise level is essentially the same as that with the tool running, indicating that the rotary tool alone does not generate appreciable electromagnetic fields in this band. In contrast, the signal strength from the spinning

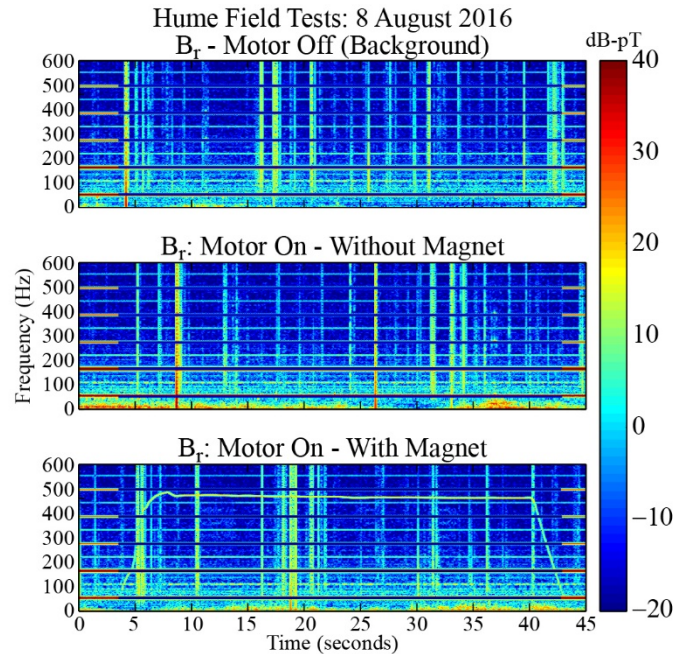


Fig. 5. Spectrograms of radial magnetic field components (B_r) measured 37 m from the source in "lighthouse" orientation: (a) rotary tool off, (b) rotary tool on without magnet present, (c) rotary tool on spinning the magnet.

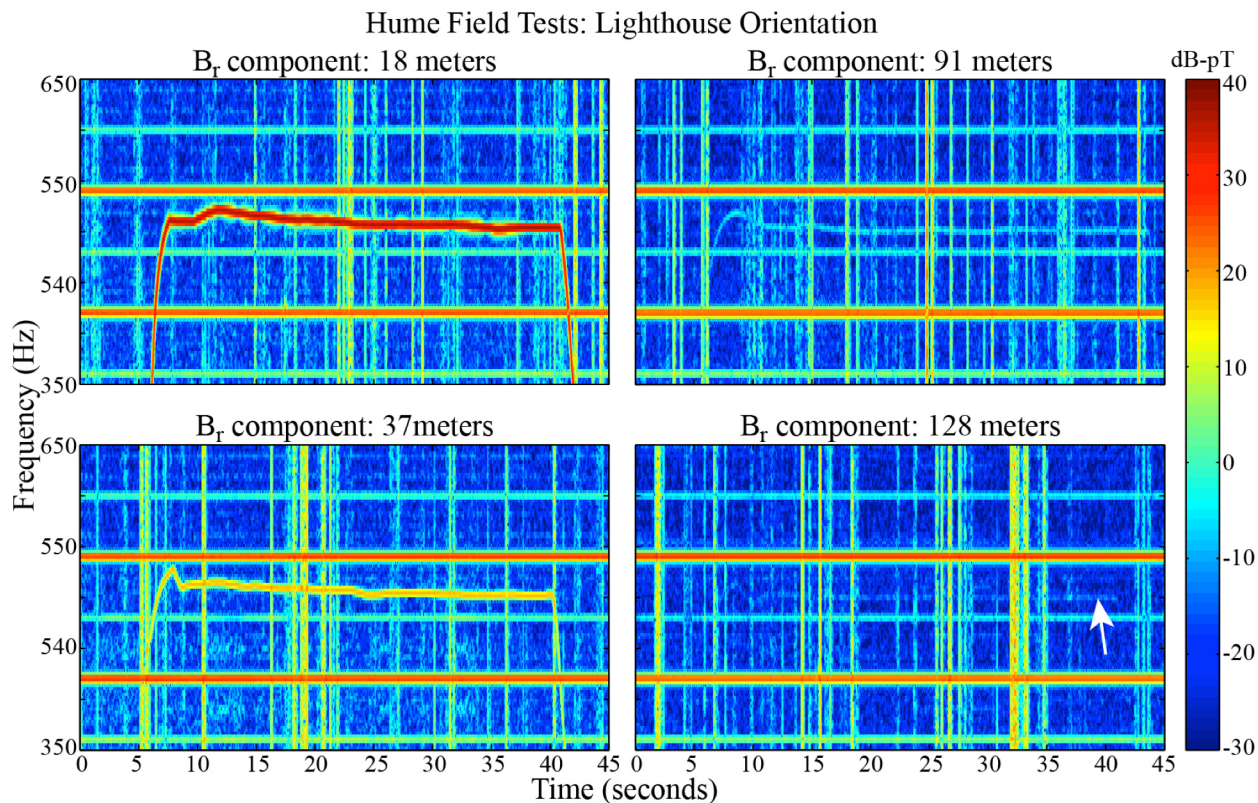


Fig. 6. Spectrograms of radial magnetic field components (B_r) measured at distances ranging from 18 m to 128 m in "lighthouse" orientation.

magnet is 25 dB-pT and is observed with ~50 dB signal-to-noise ratio. These results, and similar data collected at 9 m distance, confirm that the received signals are produced by the rotating magnet, and not by the rotary tool motor or other external interference.

It is worth mentioning that the signal strength in this small frequency range (100–500 Hz) is approximately constant with frequency, as can be seen during the ramp-up and ramp-down segments. The signal strength appears to be larger during the steady-state segment, but this visual effect is an artifact of the 2^{15} -point integration window.

B. Results with Varying Distance (Lighthouse Orientation)

Fig. 6 shows example spectrogram measurements of B_r for increasing source-to-receiver distances. The signal strength decays with distance, but clear signals are readily evident up to 91 m. Even in the 128 m case, one can observe the steady-state signal above the background. Fig. 7 summarizes the signal strength vs. distance for all three field components in lighthouse mode (log-log plot). Standard error bars derived from the noise analysis are shown, and in many cases are smaller than the marker.

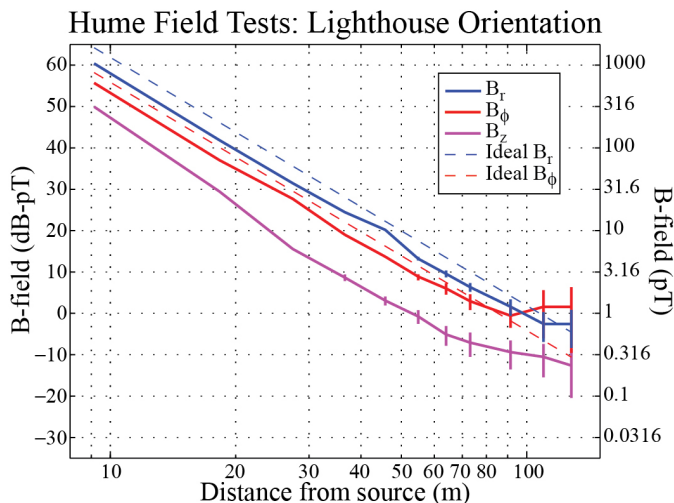


Fig. 7. Signal measurements versus distance from ELF source compared with the fields theoretically produced by a $3.1 \text{ A}\cdot\text{m}^2$ spinning magnet source over a perfectly conducting ground plane.

In Fig. 7, the data for each field component falls on a nearly straight line, indicating a power-law relationship between signal amplitude and distance. More specifically, the signal is observed to decrease with a rate of ~60 dB-pT/decade, which indicates that the magnetic field signal amplitude is decaying as $1/r^3$. This relationship matches the expected roll-off behavior of a magnetic dipole. For a single static magnetic dipole in free-space aligned with the z-axis, the B-field in spherical coordinates (r, θ, ϕ) is given as [24]:

$$B_r = \frac{\mu_0}{2\pi} M_0 \frac{\cos \theta}{r^3}, \quad B_\theta = \frac{\mu_0}{4\pi} M_0 \frac{\sin \theta}{r^3} \quad (1)$$

where M_0 is the magnetic moment of the dipole. The quasi-static fields that are produced by a rotating dipole can be calculated by assuming two orthogonally oriented dipoles that are oscillating 90° out-of-phase. Specifically, the fields

produced at the receiver location by a rotating magnet transmitter in either lighthouse orientation (x- and y-directed moments, rotating around the z-axis) or bulldozer orientation (x- and z-directed moments, rotating around the y-axis) can be calculated for two ideal cases: 1) free-space condition, and 2) perfectly conducting half-space condition (which doubles the tangential B-field and zeros the vertical B-field at the ground). The phasor-form of these ideal fields may be expressed:

Lighthouse Orientation in Free-Space:

$$B_r = \frac{\mu_0}{4\pi} M_0 \frac{1}{r^3} e^{j\pi/2}, \quad B_\phi = -\frac{\mu_0}{8\pi} M_0 \frac{1}{r^3}, \quad B_z = 0 \quad (2)$$

Lighthouse Orientation with Perfect Ground Plane:

$$B_r = \frac{\mu_0}{2\pi} M_0 \frac{1}{r^3} e^{j\pi/2}, \quad B_\phi = -\frac{\mu_0}{4\pi} M_0 \frac{1}{r^3}, \quad B_z = 0 \quad (3)$$

Bulldozer Orientation in Free-Space:

$$B_r = \frac{\mu_0}{4\pi} M_0 \frac{1}{r^3} e^{j\pi/2}, \quad B_\phi = 0, \quad B_z = -\frac{\mu_0}{8\pi} M_0 \frac{1}{r^3} \quad (4)$$

Bulldozer Orientation with Perfect Ground Plane:

$$B_r = \frac{\mu_0}{2\pi} M_0 \frac{1}{r^3} e^{j\pi/2}, \quad B_\phi = 0, \quad B_z = 0 \quad (5)$$

These equations, whether the free-space form (2) or the conducting half-space form (3), explain the $1/r^3$ dependence on distance, as well as the observed ~6 dB difference between the radial and azimuthal components shown in Fig. 7. They do not explain the relatively strong z-directed component, however, which is not 0. The non-zero z-component likely results from a combination of effects: the finite conductivity of the actual ground plane is not infinite and may vary with depth, the receiving antenna is slightly above the ground plane, rather than exactly at the ground, so that the fields do not exactly cancel, and the plane of the antenna may not be perfectly horizontal.

Evaluating the fields produced by an oscillating source above a lossy half-space is a complicated but tractable problem [26, 27]. Without knowing the properties of the lossy ground, it is reasonable to estimate that the field will behave somewhere between the free-space solution and the perfect conductor half-space solution. Using the ideal field equations, (2)–(3), the signal strengths observed in the radial direction at source distances <40 m are consistent with a source magnetic moment ranging from a lower bound of $2 \text{ A}\cdot\text{m}^2$ (assuming the perfectly conducting half-space solution) to an upper bound of $4 \text{ A}\cdot\text{m}^2$ (assuming free-space solution). This range straddles the $3.1 \text{ A}\cdot\text{m}^2$ specification of the magnet employed.

The phase difference between B_ϕ and B_r (not shown) is also reliably observed between -84° and -94° as a function of distance, nearly exactly as expected (-90°) for two phased sources representing the oscillating magnetic moment of lighthouse mode. The phase difference between B_z and B_r is more complicated: it varies from 0° at short range to -90° at large distances, likely due to the interference between the ELF source and its image in the lossy half-space.

C. Results with Different Source Orientation

Measurements comparing lighthouse (vertical) and bulldozer (horizontal) source orientations are presented in Fig.

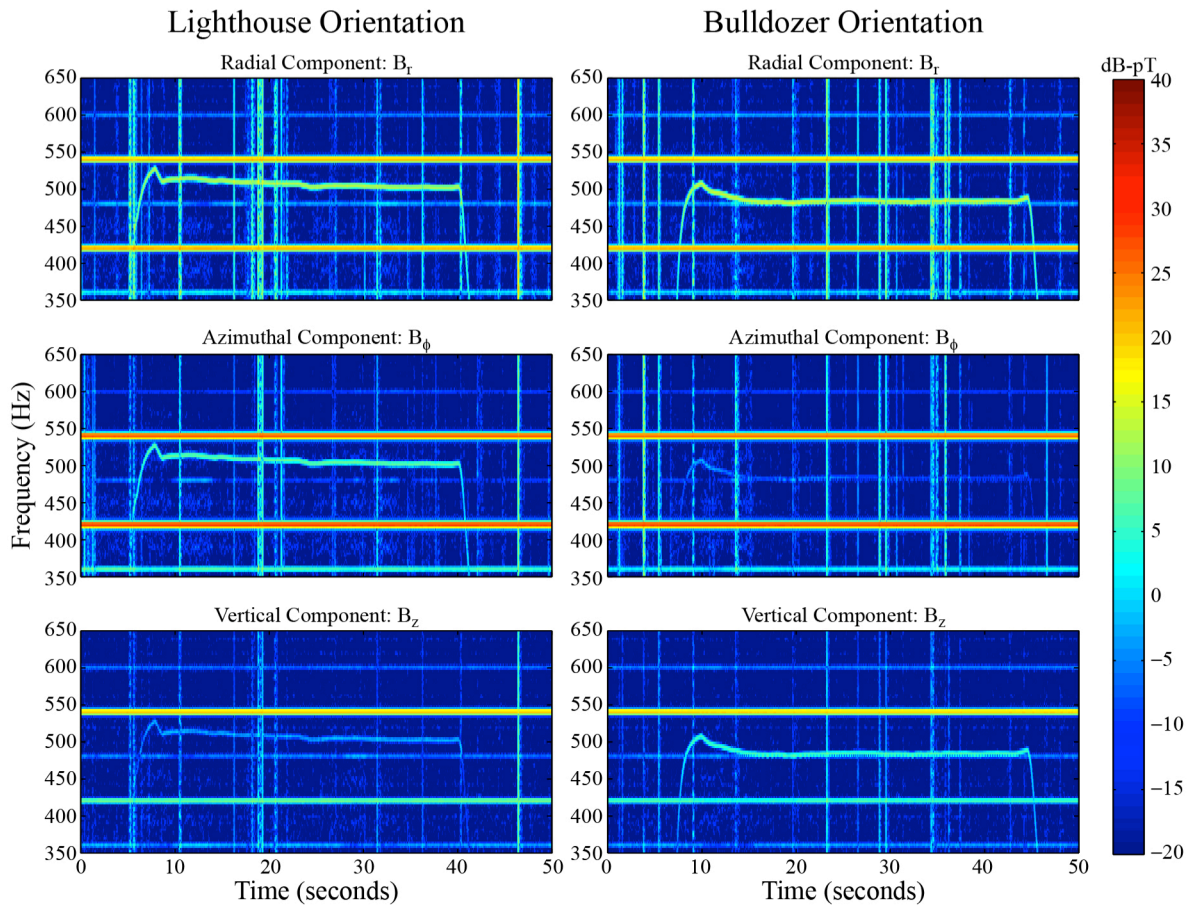


Fig. 8. Signal spectrograms for all three field components, comparing “lighthouse” and “bulldozer” magnet spin orientations at distance of 37 m.

8 and shine further light on the orientation dependence and ground-plane questions. In lighthouse mode, the amplitude of B_r is largest (25 dB-pT), followed by the B_ϕ (19 dB-pT), and then B_z (9 dB-pT). B_ϕ is 6 dB smaller than B_r , as expected in this case. The non-zero B_z component, which is 16 dB smaller than B_r , is again not consistent with either the free-space or the conducting half-space equations, (2) and (3); both predict zero vertical B-field. As described in Section III.B., the non-zero B_z component thus cannot be attributed to a finite ground conductivity. Instead, the non-zero B_z likely results from the antenna being slightly above the ground plane and not being perfectly aligned parallel to the ground.

In bulldozer mode, the amplitude of B_r is again largest (25 dB-pT), but here B_z (18 dB-pT) is larger than B_ϕ (7 dB-pT). The vertical magnetic field is significantly larger than zero, but this is not entirely unexpected, as the free-space formulation (4) contains a strong vertical component. In this case, the ground appears to be only weakly conducting so that B_z is not cancelled. Note that B_ϕ is expected to be zero for both the free-space formulation (4) and the lossy half-space formulation (5), and yet the signal is clearly detected with approximately 40 dB signal-to-noise ratio. Again, this effect is likely due to subtle offsets and misalignments in the experimental setup, along with non-uniformity in the ground plane.

To summarize, in both orientations, the largest magnetic field component is radial from the source and the smallest is parallel to the axis of rotation. Differences are also observed in the phases of the signals. An important ramification of these observed orientation effects is that the receiver may be able to determine its physical orientation relative to the source based on analysis of the vector field amplitudes.

IV. CONCLUSIONS

This work experimentally validates that time-varying magnetic fields in the ELF band can be generated by spinning magnets at the frequency of interest. In the experiments, the measured fields decayed with $1/r^3$ dependence and ranged from 58 dB-pT (~ 800 pT) at 10 m down to -2 dB-pT (~ 800 fT) at 100 m. This work suggests that communications by signaling at ELF frequencies over distances of ~ 100 m are possible by rotating a relatively small permanent magnet using a simple, compact electrical motor. Additionally, because the source produces an electromagnetic field with a certain geometric “polarization,” detection of the source orientation may also be possible via measurement of the relative strengths of the orthogonal field components.

Such compact signaling, ranging, and orienting capabilities could be very useful for data communication and/or position/navigation/timing in underground or underwater applications. In future efforts, methods for modulation and

then data encoding can also be developed. Constellations of sources could also be used for a receiver to determine its position and orientation within a given space. Arrays of receivers could also be used together with constellations of spinning magnets for specific types of imaging applications. The compact and low-power nature of the device thus provides exciting opportunities to develop new applications using ELF signals.

Further analysis is required to investigate the efficacy of this method for generating propagating electromagnetic waves in this frequency band. The fact that the experimentally evaluated dipole moment of the ELF source matches the 3.1 A·m² specification of the magnet is encouraging for the evaluation of far-field radiation. However, this dipole moment is several orders of magnitude smaller than the dipole moments associated with the conventional transmitters described in the Introduction. Assuming similar radiated power calculations [2], in order to produce 30 W of radiated power, a spinning magnet made of the same material used herein would need to be a cube of 2.5–5.0 m on a side, instead of ~1.4 cm on a side. While spinning essentially a room full of magnetic material at 100 Hz seems particularly unreasonable today, we note that many of the “conventional” ELF sources listed in the introductory section were considered unreasonable at one point in time as well.

REFERENCES

- [1] B. E. Keiser, “Early developments of the Project Sanguine radiating system,” *IEEE Trans. Comm.*, vol. 60M-22, pp. 364-371, 1974.
- [2] J. Wait, “Propagation of ELF electromagnetic waves and project sanguine/seafarer,” *IEEE Journal of Oceanic Engineering*, vol. 2, no. 2, pp. 161-172, 1977, doi: 10.1109/JOE.1977.1145337.
- [3] P. Bannister, “New simplified formulas for ELF subsurface-to-subsurface propagation,” *IEEE Journal of Oceanic Engineering*, vol. 9, no. 3, pp. 154-163, 1984, doi: 10.1109/JOE.1984.1145620.
- [4] S. L. Bernstein et al., “Long-range communications at extremely low frequencies,” *Proc. IEEE*, vol. 62, no. 3, pp. 292-312, 1974, doi: 10.1109/PROC.1974.9426.
- [5] J. Merrill, “Some early historical aspects of Project Sanguine,” *IEEE Trans. Comm.*, vol. 22, no. 4, pp. 359-363, 1974, doi: 10.1109/TCOM.1974.1092206.
- [6] E. R. Swanson, “Omega,” *Proc. IEEE*, vol. 71, pp. 1140, 1983.
- [7] U. S. Inan, D. L. Carpenter, R. A. Helliwell, and J. P. Katsfrakis, “Subionospheric VLF/LF phase perturbations produced by lightning-whistler induced particle precipitation,” *J. Geophys. Res.*, 90, 7457, 1985.
- [8] M. A. Clilverd et al., “Remote sensing space weather events: Antarctic-Arctic radiation-belt (dynamic) deposition-VLF atmospheric research consortium network,” *Space Weather*, 7, S04001, 2009, doi:10.1029/2008SW000412.
- [9] A. D. Watt, *VLF Radio Engineering*, Pergamon Press, New York, 1967.
- [10] R. Raghuram, R. Smith and T. Bell, “VLF Antarctic antenna: Impedance and efficiency,” *IEEE Trans. Antennas Propag.*, vol. 22, no. 2, pp. 334-338, 1974, doi: 10.1109/TAP.1974.1140777.
- [11] J.P. Matthews, K.H. Yearby, “Siple VLF transmissions and their magnetospheric effects observed at Halley, Antarctica,” *Advances in Space Research*, Volume 1, Issue 2, 1981, Pages 209-212, doi: 10.1016/0273-1177(81)90292-1.
- [12] P. R. Bannister, Variations in extremely low-frequency propagation parameters, *J. Atmos. Terr. Phys.*, vol. 37, pp. 1203-1210, 1975.
- [13] S. Fujimaru and R. C. Moore, “Analysis of time-of-arrival observations performed during ELF/VLF wave generation experiments at HAARP,” *Radio Sci.*, 46, RS0M03, 2011, doi:10.1029/2011RS004695.
- [14] J. Villasenor, A. Y. Wong, B. Song, J. Pau, M. McCarrick, and D. Sentman, “Comparison of ELF/VLF generation modes in the ionosphere by the HIPAS heater array,” *Radio Sci.*, 31, 211–226, 1996.
- [15] P. Stubbe, H. Kopka, and R. L. Dowden, “Generation of ELF and VLF waves by polar electrojet modulation: Experimental results,” *J. Geophys. Res.*, vol. 86(A11), 9073–9078, 1981.
- [16] A. J. Ferraro, H. S. Lee, R. Allshouse, K. Carroll, R. Lunnen, and T. Collins, “Characteristics of ionospheric ELF radiation generated by HF heating,” *J. Atmos. Terr. Phys.*, 46, 855–865, 1984.
- [17] D. S. Kotik, “ELF/VLF emissions generated in the ionosphere by heating facilities - A new tool for ionospheric and magnetospheric research,” *Radiophysics and Quantum Electronics*, vol. 37 (6), pp. 460-463, 1994, doi:10.1007/BF01088656.
- [18] R. C. Moore, U. S. Inan, T. F. Bell, and E. J. Kennedy, “ELF waves generated by modulated HF heating of the auroral electrojet and observed at a ground distance of ~4400 km,” *J. Geophys. Res.*, vol. 112, A05309, 2007, doi:10.1029/2006JA012063.
- [19] O. Cugat, J. Delamare, and G. Reyne, “Magnetic micro-actuators and systems (MAGMAS),” *IEEE Trans. Magn.*, vol. 39, no. 5, pp. 3607-3612, Nov. 2003.
- [20] J. A. Bickford, R. S. McNabb, P. A. Ward, D. K. Freeman, and M. S. Weinberg, “Low frequency mechanical antennas: Electrically short transmitters from mechanically-actuated dielectrics,” in *Proc. 2017 IEEE Symposium on Antennas and Propagation*, San Diego, CA, July 9–14, 2017, pp.1475-1476.
- [21] S. Selvin, S. Prasad M N, Y. Huang and E. Wang, “Spinning magnet antenna for VLF transmitting,” in *Proc. 2017 IEEE Symposium on Antennas and Propagation*, San Diego, CA, July 9–14, 2017, pp.1477-1478.
- [22] O. C. Fawole and M. Tabib-Azar, “An electromechanically modulated permanent magnet antenna for wireless communication in harsh electromagnetic environments,” in *IEEE Trans. Antennas and Prop.*, vol. 65, no. 12, pp. 6927-6936, Dec. 2017.
- [23] M. N. S. Prasad, Y. Huang and Y. E. Wang, “Going beyond Chu Harrington limit: ULF radiation with a spinning magnet array,” *2017 XXXIInd General Assembly and Scientific Symposium of the International Union of Radio Science (URSI GASS)*, Montreal, QC, 2017, pp. 1-3.
- [24] M. N. S. Prasad, S. Selvin, R. U. Tok, Y. Huang and Y. Wang, “Directly modulated spinning magnet arrays for ULF communications,” *2018 IEEE Radio and Wireless Symposium (RWS)*, Anaheim, CA, 2018, pp. 171-173.
- [25] J. D. Jackson, *Classical Electrodynamics*, 3rd ed. Hoboken, NY: Wiley, 2013.
- [26] A. Sommerfeld, “Über die Ausbreitung der Wellen in der Drahtlosen Telegraphie,” *Ann Phys.*, vol. 28, p. 665-736, 1909.
- [27] A. Sommerfeld, “Über die Ausbreitung der Wellen in der Drahtlosen Telegraphie,” *Ann Phys.*, vol. 81, pp. 1135-1153, 1926.



Hunter C. Burch is native to Auburn, Alabama. He earned a Bachelor of Science degree in electrical engineering from Auburn University in Auburn, Alabama in 2014, and in 2018 completed a Master of Science degree, also in electrical engineering, from the University of Florida in Gainesville, Florida.

He worked as an Undergraduate Research Assistant in the Auburn Nanotech Group at Auburn University until enrolling at the University of Florida in 2014. He is currently a Graduate Research Assistant and PhD student at the University of Florida in the Ionospheric Radio Lab. His research interests include the generation and propagation of Extremely Low Frequency and Very Low Frequency radio waves, as well as engineering applications for ELF/VLF waves such as navigation and remote sensing.

Mr. Burch is a member of the American Geophysical Union, Tau Beta Pi, and Eta Kappa Nu.



Alexandra Garraud (M'12) received the B.S. degree in electrical engineering in 2005, and the M.S. degree in applied physics in 2008, from ENS Cachan and Paris-Sud University (France). She received the Ph.D. degree in electrical engineering from Montpellier 2 University (France) in 2011, with a support from a ENS Cachan fellowship.

She is currently a research assistant professor in the Electrical and Computer Engineering department at the University of Florida. Her research interests include the fabrication, the development and the characterization of ferromagnetic and ferroelectric materials and microsystems for power and low-power memories applications.



Robert C. Moore (M '07–SM '18) received his B.S., M.S., and Ph.D. degrees in electrical engineering from Stanford University, Stanford, CA in 1999, 2001, and 2007, respectively.

He is currently an Associate Professor at the University of Florida in the Department of Electrical and Computer Engineering. He actively conducts research on lightning, high power radio wave interactions in the ionosphere, ELF/VLF remote-sensing, and engineering applications of low frequency radio wave propagation.

Dr. Moore currently serves as chair of Commission H (Waves in Plasmas) for the U.S. National Committee for the International Union for Radio Science (URSI) and as chair of the RF Ionospheric Interactions Workshop Steering Committee.



David P. Arnold (S'97–M'04–SM'10) received dual B.S. degrees in electrical and computer engineering in 1999, followed by the M.S. degree in electrical and computer engineering in 2001, from the University of Florida, Gainesville. He received the Ph.D. degree in electrical and computer engineering at the Georgia Institute of Technology, Atlanta in 2004.

Currently, he is the George Kirkland Engineering Leadership Professor in the Department of Electrical and Computer Engineering at the University of Florida, Deputy Director of the NSF Multifunctional Integrated System Technology (MIST) Center, and Director of the UF Interdisciplinary Microsystems Group (IMG). He has co-authored over 180 refereed journal and conference publications, and holds 18 U.S. patents. His research focuses on micro/nanostructured magnetic materials, magnetic microsystems, electromechanical transducers, and miniaturized power/energy systems.

Dr. Arnold's research innovations have been recognized by the 2008 Presidential Early Career Award in Science and Engineering (PECASE) and the 2009 DARPA Young Faculty Award. He is an active participant in the magnetics and MEMS communities, with ongoing involvement in various conference committees and currently serving on the editorial boards of *J. Micromechanics and Microengineering* and *Energy Harvesting and Systems*. He is also a member of Tau Beta Pi and Eta Kappa Nu.